Performance of Smart Revenue Meters Under Bidirectional Active Energy Flows in Energy Communities

Jan Klusacek, *Student Member, IEEE*, Roberto Langella, *Senior Member, IEEE*, Jan Meyer, *Senior Member, IEEE*, and Jiri Drapela, *Senior Member, IEEE*

***Abstract*— Bidirectional active energy flows are expected to increase in electrical distribution systems (DSs) worldwide as a result of future incentives to exchange energy within local energy communities. Distributed generation (e.g., solar rooftop photovoltaic systems) in combination with full-cycle pulsewidth regulated loads (e.g., thermal appliances or some energy diverters), battery storage systems, or regenerative loads will result in periodic changes in the energy flow direction. If the regulation periods are close to the aggregation time window of smart revenue meters (RMs), the deviation from the correct readings of export and import registers might be significant. Subsequently, economic transactions that rely on readings from RMs, especially in community grids, might fail. The article presents an overview of the active power and energy metrics that are either already being implemented in static RMs or derived from other applications of active power measurement. A parametric analysis and an experimental case-study demonstrated quantitatively that different metrics and different influencing factors/conditions can lead to large deviations in the readings of RMs in community grids, causing significant technical and financial consequences. Finally, a new testing procedure capable of verifying the susceptibility of RMs to these quickly changing bidirectional energy flows is proposed and experimentally demonstrated with the goal of including it in future updates of the relevant standards.**

***Index Terms*— Active energy metrics, active power metrics, bidirectional power flow, energy community, energy exchange, revenue metering, smart meters, watthour meters.**

I. Introduction

DURING the massive development of electrical distribution systems (DSs) worldwide in the second half of the 20th century, revenue metering became increasingly important to ensure fair remuneration for energy generation and the allocation of distribution costs to the end-users [1]. Historically, the energy flow was prevalently unidirectional, i.e., energy was generated in large generating plants and distributed to the end-users. Thus, the concept of energy registration for billing was developed based on simple assumptions, some of which are no longer valid. For instance, in the context of dynamic changes in the power at the point of measurement (PoM), the paradigm assumed that even if a load generates power on a short-term basis (e.g., the generator mode of an electrical motor), the energy export is part of the process behind the meter and might be ignored (e.g., the disk brake in an electromechanical meter) [2].

However, the development of distributed generating plants in recent decades has changed the paradigm of DSs. The energy flow is typically intentionally diverted in the prosumers' installations behind their revenue meters (RMs) [3], [4] in a local energy community [5], or on the scale of a grid-tie microgrid [6], leading to bidirectional energy flows. Such changes in the energy flow direction may be periodic as a result of the concurring operation of a generating power plant and an energy divertor with specific hardware [7] providing full-cycle pulsewidth regulation (PWR). PWR is typically utilized for appliances controlling thermal loads (e.g., cooking appliances, air conditioners, air heaters, and water heaters). The periodic changes in the energy flow direction in modern installations might also be caused by unstable control loops of commercial battery storage systems [8], or power alternations of a recuperating elevator (i.e., a green lift) [9] and [10]. All cases documented long-term bidirectional active energy flows between a user installation and DS with a lower or higher rate of intentional/non-intentional active energy direction changes.

Because of citizen participation in all markets, either by generating, consuming, sharing, or selling electricity, the market platforms for local energy trading, including peer-to-peer trading, are currently being developed and tested worldwide within local energy communities [11], [12]. For any business model adopted, the use of bidirectional RMs capable of separately registering positive and negative energy flows will be crucial in all circumstances. This will be the case both at a prosumer's point of connection (PoCs) and at the PoM, where a local energy community grid ("community

Manuscript received 12 December 2023; revised 4 March 2024; accepted 12 March 2024. Date of publication 28 March 2024; date of current version 11 April 2024. This work was supported by the Specific Research Program under Project FEKT-S-23-8403. The Associate Editor coordinating the review process was Dr. Ferdinanda Ponci. *(Corresponding author: Roberto Langella.)*

Jan Klusacek and Jiri Drapela are with the Department of Electrical Power Engineering, Faculty of Electrical Engineering and Communication, Brno University of Technology, 612 00 Brno, Czech Republic (e-mail: klusacekj@vut.cz; drapela@vut.cz).

Roberto Langella is with the Department of Engineering, University of Campania "Luigi Vanvitelli," 81031 Aversa, Italy (e-mail: roberto.langella@unicampania.it).

Jan Meyer is with the Institute of Electrical Power Systems and High Voltage Engineering, TUD Dresden University of Technology, 01069 Dresden, Germany (e-mail: jan.meyer@tu-dresden.de).

Digital Object Identifier 10.1109/TIM.2024.3382732

grid" in what follows) is connected to a DS. Moreover, the correct measurement of active power is decisive for novel grid-operation concepts, which use the data from RMs, e.g., for controlling the community grid [13], system monitoring [14], and including unbalanced conditions [15].

The fundamental requirements for RMs in the EU, especially in the context of static RM development, are formulated in the EU Directive [16] and further specified in the EN 50 470 family of standards (i.e., −1 [17] and −3 [18] for static RMs). At the international level, general and specific requirements are set by the IEC 62 052 [19] and IEC 62 053 [20] groups of standards, respectively. Data exchange is standardized in the IEC 62 056 series [21], where the registers of measured quantities, including active energy import and export registers, are defined. The standards [17], [18], [19], [20] do not contain the definition of active energy and how to measure it, but specify tests to verify the accuracy of RMs under reference and influencing conditions.

The influencing conditions, coming from real DSs, are further discussed in the literature, which reports the results when meters were exposed to non-ideal power quality conditions [22] including harmonic distortion [23], [24], and dynamic variations [25], [26]. However, to the best of our knowledge, the ability of RMs (on individual outputs) to distinguish energy import and export under fast (frequent) changes in the power direction (e.g., as a result of active energy management in a prosumer's installation behind their meter) has not been considered; except a preliminary work from some of the authors [3].

The lack of standardization of a measurement method has driven the use of different energy measurement metrics [27], [28], [29], [30], which obviously means that their response may vary under non-standardized tests. For instance, the active power algorithm based on the classical definition of active power (1) inherently gives the average over the period T [3]. On the other hand, although algorithms based on eliminating the instantaneous power oscillating part [28], [29], [30] can be derived from (1) in the steady state, the instantaneous results differ during dynamic changes in the active power. In the presence of periodic "bidirectional" active power changes with a period close to or even shorter than T, the definition of active power might be rather ambiguous [31].

This article extends the results reported in [31], which discussed the ability of RM metrics to correctly register bidirectional active energy flows in active distribution networks.

The objective of this article is to identify and quantify the relative deviations associated with different measurement results from RMs that use different metrics, both at different PoMs and for individual outputs of a single RM. After the introduction, in Section II, a brief overview of the active power and energy metrics that are either already being implemented in static RMs or derived from other applications of active power measurement is done. In Sections III and IV, a parametrical analysis of the metrics' performances for different variants of both the active power flows and metrics' settings is performed numerically and experimentally, respectively. In Section V, a general discussion of the results obtained and some recommendations are given. Finally, Section VI reports

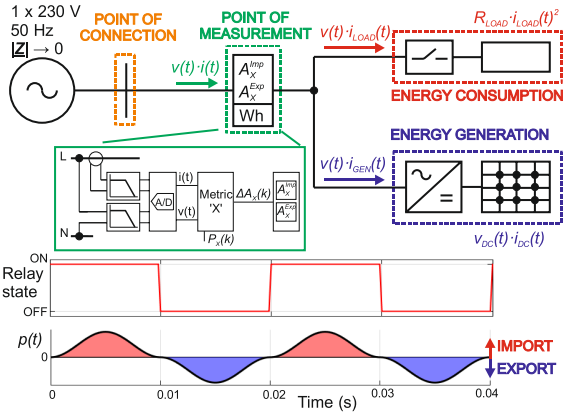

Fig. 1. Single line diagram of a prosumer with a generator and switching load causing periodic and fast changes in the active power direction at the PoM/PoC.

and new testing procedure aimed at verifying the susceptibility of RMs to fast-changing bidirectional energy flows, experimentally demonstrated and recommended to include in future updates of the relevant standards.

II. Metrics for Active Power and Energy

This section presents and describes selected algorithms (metrics) used for single-phase circuit active power and energy calculation in detail. Each metric uses sampled voltage and current waveforms as inputs, which, in a real application, would be the outputs of a measuring chain consisting of voltage and current transducers, analog front-ends, and analog-to-digital (A/D) converters. This section and Section III assume that this measuring chain is ideal and not affected by uncertainties.

A. Bidirectional Active Power Measurement and Active Energy Registration Theory

The common definition of the active power, P, based on instantaneous voltage and current, $v(t)$ and $i(t)$, respectively, expresses the active power as an average rate of energy exchange (i.e., active energy A) during a specific period of time, T [13], [17], and in consecutive measuring intervals, k

$$P(k) = \frac{1}{T}\int_{t(k)}^{t(k)+T} v(t)\cdot i(t)\cdot dt \tag{1}$$

$$A(k) = P(k)\cdot T. \tag{2}$$

Under a bidirectional active energy exchange, the active energy import or export, based on the sign of $P(k)$ and/or $A(k)$, can be recognized more or less correctly if the period of the changes is much longer than T.

With reference to Fig. 1, assume that an installation has a permanently operating generator of constant active power and, at the same time, a permanently connected load absorbing twice its active power. The load is, however, periodically switched on for half of each fundamental cycle ($T_{\text{fund}}/2$). Under these conditions, the direction of the active power in the PoM will change periodically every half cycle, and its average value per switching cycle ($T_{\text{sw}} = T_{\text{fund}}$) will be zero. Therefore, zero active power and energy is calculated if T in (1) and (2) is equal to T_{fund}. This phenomenon may become issue if

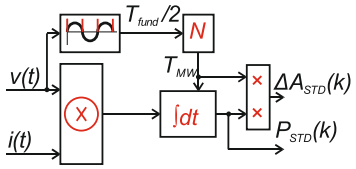

Fig. 2. Signal diagram of the STD metric.

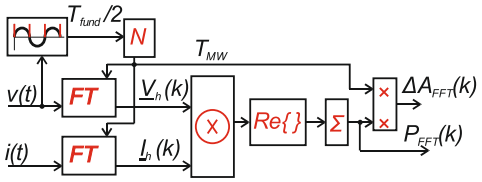

Fig. 3. Signal diagram of the FT metric.

the sorting of imported and exported energy is legitimately required [3] as it will be further analyzed in Section III.

The outputs of each of the metrics described in Sections II-B–II-F are the active power, $P_X(k)$, and active energy increment, $\Delta A_X(k)$, where X denotes the metric type considered. The $\Delta A_X(k)$ value is then sorted to the import register (Imp) or export register (Exp), according to its sign in (3) and (4). Hence, the increment is added to the total exported $A_X^{\mathrm{Exp}}(k)$ or imported $A_X^{\mathrm{Imp}}(k)$ energy

$$A_X^{\mathrm{Imp}}(k) = A_X^{\mathrm{Imp}}(k-1) + \left\{ \begin{array}{ll} 0; & if\, \Delta A_X(k) < 0 \\ |\Delta A_X(k)|; & if\, \Delta A_X(k) \geq 0 \end{array} \right\} \tag{3}$$

$$A_X^{\mathrm{Exp}}(k) = A_X^{\mathrm{Exp}}(k-1) + \left\{ \begin{array}{ll} 0; & if\, \Delta A_X(k) \geq 0 \\ |\Delta A_X(k)|; & if\, \Delta A_X(k) < 0 \end{array} \right\}. \tag{4}$$

B. Standard (STD) Metric

The signal diagram of the STD metric is shown in Fig. 2. The voltage and current signals are first multiplied to obtain the instantaneous power. Subsequently, the instantaneous power is integrated over the interval of measuring window T_{MW}, which has a length equal to an integer multiple N of the system fundamental frequency half-period, $N \cdot T_{\mathrm{fund}}/2$. The active power can be calculated as follows:

$$P_{\mathrm{STD}}(k) = \frac{1}{T_{\mathrm{MW}}} \int_{t(k)}^{t(k)+T_{\mathrm{MW}}} v(t) \cdot i(t) \cdot dt. \tag{5}$$

Various methods can be used to track the fundamental period. This article considers a method based on voltage zero crossings.

Finally, the active energy increment, $\Delta A_{\mathrm{STD}}(k)$, is calculated

$$\Delta A_{\mathrm{STD}}(k) = T_{\mathrm{MW}} \cdot P_{\mathrm{STD}}(k). \tag{6}$$

C. FT-Based Metric

The signal diagram of the Fourier transform (FT) metric is shown in Fig. 3. First, the FT is applied to voltage and current waveforms with a length of T_{MW}. The active power, $P_{\mathrm{FT}}(k)$, is then calculated

$$\left[\underline{V}(h)\right] = \mathcal{F}\left(v(t)_{T_{\mathrm{MW}}}\right), \left[\underline{I}(h)\right] = \mathcal{F}\left(i(t)_{T_{\mathrm{MW}}}\right) \tag{7}$$

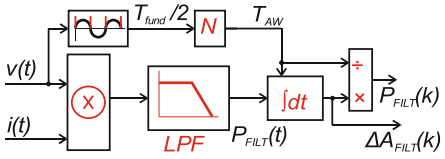

Fig. 4. Signal diagram of the FILT metric.

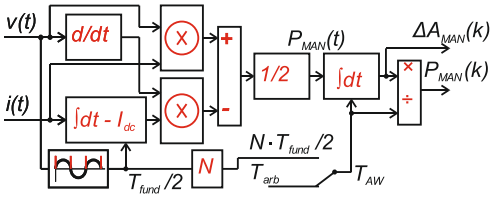

Fig. 5. Signal diagram of the MAN metric.

$$P_{\mathrm{FT}}(k) = \sum_{h=1}^{H} \mathrm{Re}\left\{\underline{V_h} \cdot \underline{I_h}\right\} \tag{8}$$

where H is the highest harmonic order, h, considered (typically $H = 25$ for RMs). The value of $\Delta A_{\mathrm{FT}}(k)$ is then calculated as follows:

$$\Delta A_{\mathrm{FT}}(k) = T_{\mathrm{MW}} \cdot P_{\mathrm{FT}}(k). \tag{9}$$

The measurement window is $T_{\mathrm{MW}} = 20 \cdot T_{\mathrm{fund}}/2$ and the fundamental period is estimated like in the STD case.

D. Filter-Based (FILT) Metric

The signal diagram of the FILT metric is shown in Fig. 4 [28]. The voltage and current waveforms are first multiplied to obtain the instantaneous power. The instantaneous power is then filtered using a low-pass filter (LPF), or alternatively, a band stop notch type filter (BSF) tuned to double the nominal system frequency (e.g., 100 Hz for 50 Hz systems). The energy increment, $\Delta A_{\mathrm{FILT}}(k)$, is calculated as in (10), where the symbol "$*$" denotes convolution and T_{AW} is the smoothing time interval, which practically might be as small as the discrete signal sampling interval. Regarding the finite attenuation of the filter, resulting in a residual ~100 Hz ripple of $P_{\mathrm{FILT}}(t)$, it is advantageous to set the average window length, T_{AW}, as an integer multiple of $T_{\mathrm{fund}}/2$. Because the ripple of instantaneous power p is naturally linked with double the fundamental frequency, $T_{\mathrm{AW}} = T_{\mathrm{fund}}/2$ is considered. Thus, the residual ripple is eliminated in the sequence of consecutive $\Delta A_{\mathrm{FILT}}(k)$ values

$$\Delta A_{\mathrm{FILT}}(k) = \int_{t(k)}^{t(k)+T_{\mathrm{AW}}} (h * p)(t) \cdot dt$$
$$h(t) = \mathcal{L}^{-1}\{F_{\mathrm{FILT}}(s)\},\ p(t) = v(t) \cdot i(t). \tag{10}$$

The active power, $P_{\mathrm{FILT}}(k)$, is calculated as follows:

$$P_{\mathrm{FILT}}(k) = \Delta A_{\mathrm{FILT}}(k)/T_{\mathrm{AW}}. \tag{11}$$

E. Manipulation (MAN) Metric

The signal diagram of the MAN metric is shown in Fig. 5 [29]. The voltage waveform is first differentiated, and then the current waveform is integrated. In principle, the current waveform could be differentiated, and the voltage integrated. However, the derivation is applied to the voltage to avoid high

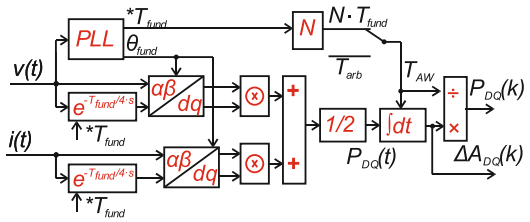

Fig. 6. Signal diagram of the DQ metric.

derivation values due to steep slopes and rapid changes in current. Consequently, instantaneous power $p(t)$ and component $p'(t)$ are obtained (12), (13) as follows:

$$p(t) = v(t) \cdot i(t) \tag{12}$$

$$p'(t) = \frac{dv(t)}{dt} \cdot \left[\int_{t(k)}^{t(k)+T_{\text{fund}}} i(t)dt - I_{\text{dc}} \right]. \tag{13}$$

Practically, integration constant I_{dc} represents a dc component of the current and is eliminated in the algorithm [see the square brackets in (13)]. The value of I_{dc} might be calculated as the average of $i(t)$ over T_{fund}, or by filtering using the LPF or BSF (15). In the case of (14), the current integration is performed over a single T_{fund}. Therefore, the fundamental period must be tracked, e.g., by means of voltage zero-crossing detection as in previous metrics. On the other hand, system frequency tracking might be avoided by applying (15)

$$I_{\text{dc}} = \frac{1}{T_{\text{fund}}} \int_{t(k)}^{t(k)+T_{\text{fund}}} i(t)dt \tag{14}$$

$$I_{\text{dc}} = (h * i)(t), h(t) = L^{-1}\{F_{\text{MAN}}(s)\}. \tag{15}$$

The output active power, $P_{\text{MAN}}(t)$, represents the active power in each instant of time (16), i.e., in each sampling interval in the case of its discrete form

$$P_{\text{MAN}}(t) = 1/2 \cdot \big(p(t) - p'(t)\big). \tag{16}$$

The output active energy increment, $\Delta A_{\text{MAN}}(k)$, and active power, $P_{\text{MAN}}(k)$, can be obtained by integration over time period T_{AW}, as in (11) for FILT. Unlike for FILT, however, T_{AW} does not necessarily have to be an integer multiple of the fundamental half-period ($N \cdot T_{\text{fund}}/2$), but an arbitrary integration period could be selected (T_{arb}). In this case, T_{arb} is selected, which is the same as the sampling interval of the input signals. Thus, $\Delta A_{\text{MAN}}(k)$ is calculated for every (discrete) instant.

F. D-Q Frame (DQ)-Based Metric

A DQ-based metric has been derived from a single-phase inverter control algorithm as an alternative to previous metrics employed by real-life RMs, as shown in Fig. 6 [30]. The fundamental component of the metric is obtained by means of a phase-locked loop (PLL) algorithm, which tracks the voltage instantaneous angle. The angle is then used for Park transformation to obtain the voltage and current components of a synchronous d-q frame (v_d, v_q and i_d, i_q, respectively).

$P_{\text{DQ}}(t)$ (17) represents the active power in every instant of time, i.e., the sampling interval in a real application

$$P_{\text{DQ}}(t) = \frac{1}{2} \cdot \left(v_d \cdot i_d + v_q \cdot i_q\right). \tag{17}$$

Moreover, the output active energy increment, $\Delta A_{\text{DQ}}(k)$, and active power, $P_{\text{DQ}}(k)$, can be obtained by integration over time period T_{AW}, which might not necessarily be an integer multiple of $T_{\text{fund}}/2$, but it may be any multiple of the sampling interval, T_{arb}. In this study, the value of T_{arb} selected was the same as the sampling interval of the input signals.

The PLL estimates both voltage instantaneous angle $\Theta_{\text{fund}}(t)$ and fundamental period T_{fund}, which is used: 1) for shifting the input waveforms by $T_{\text{fund}}/4$ and 2) for calculating $P_{\text{DQ}}(k)$ and $\Delta A_{\text{DQ}}(k)$ if the measuring interval (T_{AW}) of the kth energy increment is synchronized with $T_{\text{fund}}/2$.

III. Parametrical Analysis

In this section, the performances of the metrics are analyzed under periodic changes in the direction of the active power, comparing the output active power ($P_X(k)$) and total registered energy ($A_X(k)$) with the true reference values while changing the parameters of both the active power flows and metrics.

A. Test Specifications

With reference to Fig. 1 the true active power was alternated between −2300 and +2300 W with frequency f_{sw} to emulate the resulting power of a generating unit (2300 W) and switching load (4600 W), which achieved a zero average power in a switching cycle of length $T_{\text{sw}} = 1/f_{\text{sw}}$, with a duty cycle, D, equal to 0.5. T_{sw} was varied from a fractional 0.05th multiple to the integer 500th multiple of fundamental period T_{fund}. In the tested 50 Hz system, this provided f_{sw} values in range of 0.1–1000 Hz, using 0.1 Hz steps in the range of 0.1–100 Hz and 10 Hz steps in the range of 100–1000 Hz. The value of f_{sw} was varied to keep T_{sw} as an integer divisor of the testing signal total length (i.e., 10 s) to avoid bias in the Imp and Exp registers as a result of unequal consumed and generated energy values over the observation period. The active energy increments were sorted according to (3) and (4).

Parametric modifications of the metrics are as follows: STD1/2p, STD10p, and STD50p stand for STD variants implementing $T_{\text{MW}} = \{0.5, 10, 50\} \cdot T_{\text{fund}}$. FT metric has only a single variant FT10p, $T_{\text{MW}} = \{10\} \cdot T_{\text{fund}}$, being the typical time window of FT in Power Analyzers and because it gives the same results of STD. FILT LPF6 Hz, FILT LPF100 Hz, and FILT BSF100 Hz stand for FILT variants differing by the applied filter (LPF or BSF) and stopband frequency (f_{stop}). For example, FILT LPF6 Hz implements LPF with $f_{\text{stop}} =$ 6 Hz and represents the recommended setting for the dynamic measurement of active power [28]. FILT LPF100 Hz and FILT BSF100 Hz with $f_{\text{stop}} = 100$ Hz represent settings to filter double the fundamental frequency component at 50 Hz. MAN int, MAN BSF, and MAN LPF are variants of MAN and implement different methods to eliminate integration constant I_{dc} (13).

B. Results

Fig. 7 shows active power P_X versus time provided by each metric for switching cycle $T_{\text{sw}} = 0.12$ s (i.e., $6 \cdot T_{\text{fund}}$, $D = 0.5$, $f_{\text{sw}} = 8.33$ Hz); the blue solid line represents the reference.

The window-based metrics (STD50p, STD10p, and FT10p) evidently average the active power in the measurement

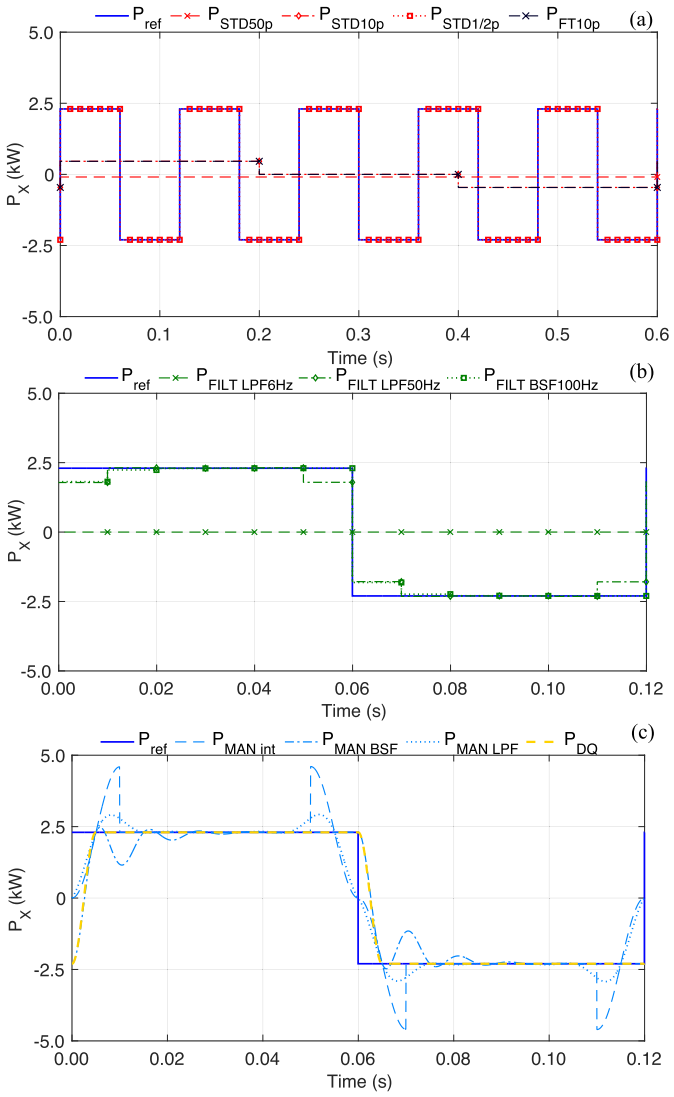

Fig. 7. Active power provided by the metrics in the measurement intervals under active power direction changes ($D = 0.5$) with $T_{sw}/T_{fund} = 6$. (a) Reference (P_{ref}), STD and FT metrics. (b) P_{ref} and FILT metric. (c) P_{ref}, MAN and DQ metrics.

window, which leads to a cyclic error with a period of 0.6 s in the STD10p and FT10p cases because T_{sw} is a non-integer divisor of T_{MW} [see Fig. 7(a)]. STD1/2p is very accurate, while STD50p measures almost zero active power as a result of its long averaging window.

The step-wise behaviors of all the FILT metrics indicate the presence of the $T_{fund}/2$ averaging window [see Fig. 7(b)]. FILT LPF100 Hz provides lower values both before and after every change in the true active power, whereas FILT BSF100 Hz exhibits lower active power after the change. FILT LPF6 Hz measures zero because f_{sw} is over the filter cut-off frequency.

The MAN metrics (MAN int, MAN LPF, and MAN BSF) and DQ provide relatively accurate results for every sampling interval. However, each parametric variant exhibits a different overshoot [see Fig. 7(c)]. MAN int and MAN LPF show the overshoot before and after the change symmetrically. In contrast, MAN BPF shows the overshoot exclusively after the change. The DQ metric provides results for every sampling interval without overshoot. However, they have a delay compared to the reference, P_{ref}.

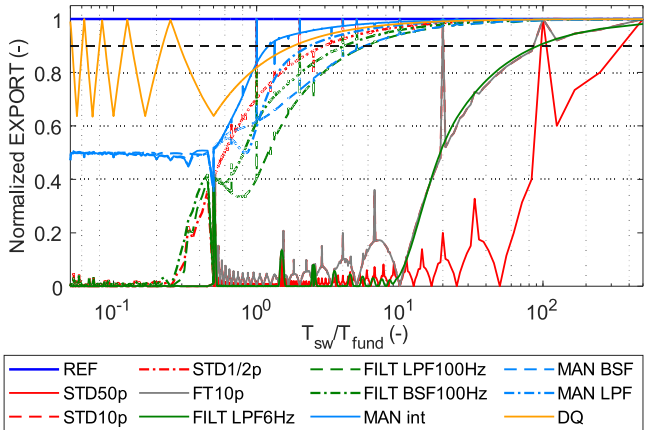

Fig. 8. Normalized active energy values registered by the metrics in the export register ($D = 50\%$).

The ability of each metric to register the exported energy at PoM is visualized in Fig. 8. The complement to one of the curves shown can be considered the metric's deviations (i.e., errors). Every test point corresponds to the final value of A_X^{Exp} in the last measuring interval, k, of the testing interval with the specific T_{sw} that is normalized to T_{fund}. The energy registered in the Exp register has been normalized by reference values, which were calculated as integrals of the negative values of the instantaneous power versus time. Thus, the results are normalized to the exact amount of active energy, which is evidently exchanged with DS via PoM. For instance, the reference export for $T_{sw}/T_{fund} = 0.5$ was obtained as the sum of the blue areas, similar to Fig. 1, and applied to the 10 s signal. Because the switching duty cycle was 50% and the energy balance during each T_{sw} was zero, the absolute values of A_X^{Exp} and A_X^{Exp} are equal, i.e., Fig. 8 also applies to the import register.

Fig. 8 also shows that STD10p and FT10p had similar behaviors because both used the same time window for calculation ($10{\cdot}T_{fund}$), with the energy increments stored in the corresponding register. FILT LPF6 Hz could not recognize the changes with f_{sw} lower than 5 Hz ($T_{sw}/T_{fund} = 10$). However, the peaks in the registered energy at $T_{sw}/T_{fund} < 10$ indicate the smoothing window, T_{AW}. Although STD50p, STD10p, and FILT LPF6Hz represent widely utilized metrics in commercial RMs, it can be seen that they practically register the energy correctly if the frequency of the changes (i.e., T_{sw}) is on the order of seconds (T_{sw} =10 s means $T_{sw}/T_{fund} = 500$, see Fig. 8). However, the performance of STD and FILT strongly depend on the T_{MW} length and filter design, respectively; e.g., FILT LPF6Hz shows significant deviations (>10%) if $T_{sw}/T_{fund} < 90$ in a 50 Hz system but the same deviation is achieved at $T_{sw}/T_{fund} < \{6, 4\}$ in the cases of FILT LPF100 Hz and FILT BSF100 Hz, respectively. STD10p achieves the same error at $T_{sw}/T_{fund} < 80$, while STD1/2p shows it even at $T_{sw}/T_{fund} < 3$. On the other hand, MAN shows comparably low deviations when $T_{sw}/T_{fund} \geq 0.5$ and settles at 50% at $T_{sw}/T_{fund} \leq 0.5$, regardless of the parametric variation (MAN int, MAN LPF, MAN BSF).

The DQ metric error ranges between 0% and 37% in the whole range, being the smallest error among the metrics. For $T_{sw}/T_{fund} < 0.5$, however, the error is minimum if

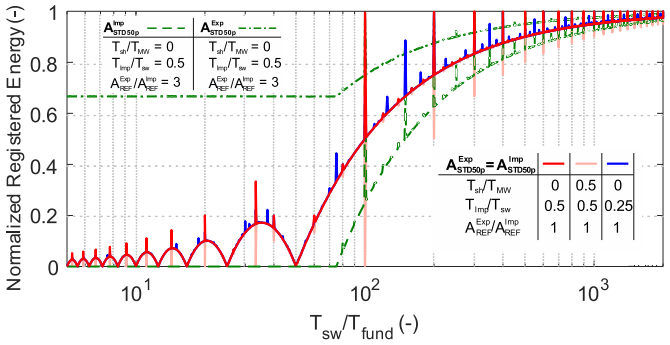

Fig. 9. Registered energy values of STD50p under various influencing conditions at PoM.

$T_{sw}/T_{fund} = \{1/20, 1/16, 1/12, 1/8, 1/4\}$ and maximum if $T_{sw}/T_{fund} = \{1/18, 1/14, 1/10, 1/6, 1/2\}$.

C. Other Influencing Conditions

Fig. 8 summarizes the results for test scenarios when the switching D was 50% and the real imported and exported energy values were the same within each cycle. Moreover, the measuring and averaging windows, in the case of the STD and FILT metrics, started with the switching cycle (i.e., with the change in the switch state).

As shown in a theoretical study [3] of the STD and FT metrics, a variation in these aspects may change the energy registration ratios with implications for curves like those shown in Fig. 8. The following parameters have an influence: 1) the duration of the energy import, T_{Imp}, within T_{sw}, in ratio T_{Imp}/T_{sw} (corresponding to the duty cycle, D); 2) balance between the real exported and imported energy values during T_{sw}, in ratio $A^{Exp}_{REF}/A^{Imp}_{REF}$; 3) time shift, T_{sh}, between the beginning of the switching cycle and measuring window, expressed as T_{sh}/T_{MW}. The third parameter has an obvious effect on the MW and AW based on the employed metrics (i.e., STD, FT, and FILT) when SW and MW are synchronized, while the second parameter changes the relative results of any metric.

Fig. 9 reports the effects in the case of STD50p due to the following variants of the influencing conditions (the same as the experimental case study presented in Section IV): $A^{Exp}_{REF}/A^{Imp}_{REF} = \{1,3\}$;$T_{Imp}/T_{sw} = \{0.5,0.25\}$; and $T_{sh}/T_{MW} = \{0,0.5\}$. It is evident that ratio $A^{Exp}_{REF}/A^{Imp}_{REF}$ has the major impact on the accuracy of the results.

IV. Experimental Case Study

The consequences of the metric deviations under dynamic changes in the active energy flow direction in a minimalistic energy community were experimentally analyzed. The test system was a minimal setup for billing between the end-users and the community grid and between the community grid and DS operator (DSO).

A. Experimental Setup

Fig. 10 shows the system considered. It was connected to an upstream utility grid operated by a DSO in a single PoC (FEED), with one prosumer (PRO) and one consumer (CON), connected at PoC PRO and PoC CON, respectively. The RMs were located at PoCs FEED, PRO, and CON.

The PRO had a PV generation unit (3 kW@230 V) and switched resistive load (4 kW@230 V) in the PWR mode and intended to sell the excess energy to the CON, who had a constant resistive load (1 kW@230 V). The utility grid was emulated by a grid simulator (Spitzerberger DM 45000/PAS).

The alternation between energy Import and Export at the PoC PRO was achieved by a combination of: 1) a PV inverter connected to a PV array simulator (Spitzerberger PVS 7000), delivering 3.185 kW that resulted in 3 kW at the inverter ac front-end; and 2) a 13.23 Ω resistor for the nominal power, 4 kW@230 V. The resistor was switched using a triac with a specific switching function, where cycle length T_{sw} was an integer multiple of $T_{fund}/2$ ($D = 0.5$), synchronized with a voltage zero-crossing. Consequently, the power at the PoC PRO alternated between −3 and 1 kW. The f_{sw} value of the triac was varied across discrete values, {10, 2.5, 1.25, 1, 0.625, 0.55, 0.5, 0.43, 0.2, 0.12, 0.03} Hz, leading to $T_{sw} \simeq$ {0.1, 0.4, 0.8, 1, 1.6, 1.82, 2, 2.33, 5, 8.33, 33.33} s in ten consecutive tests. The consumption at the PoC CON was simulated using a 52.9 Ω resistor for a nominal power of 1 kW@230 V in all the tests. Each test lasted approximately 1 h. Therefore, the expected resolution uncertainty of all the RMs used was within 1/10 of their accuracy class.

Three different off-the-shelf meters for individual PoMs were used (real rms), all with valid certifications and accuracy class A. The registered energy in the RM at the PoC FEED could be read from different outputs (LED pulse output, electrical pulse outputs PO+/PO-, and Imp/Exp cumulative registers). In the case of the LED and PO+/PO−, the reading was done by counting the pulses, where the constants were 500 (LED) and 250 (PO) pulses/kWh. On the other hand, the Imp/Exp registers in all the RMs were accessible via optical or electrical interfaces using specific communication protocols [32].

Throughout this section, $A^{Y}_{X,Z}$ represents the energy registered by method X in register Y and PoC Z. The Z represents {PRO, CON, FEED} and X is {RM, REF, STD50p, STD10p, STD1/2p}, where RM stands for readings from an off-the-shelf RMs for billing, REF stands for a calculated reference, and STD50p, STD10p, and STD1/2p stand for the emulated metrics – modeled RMs (as implemented in Section III, and deployed for comparison). Both the REF and STD post-processes sensed and recorded instantaneous voltage and current signals. Finally, Y represented {Imp, Exp, PO+, PO−, LED}.

The setup was designed to achieve a reference energy ratio export/import of approximately 3 at the PoC PRO to simulate the exporting nature of PRO. CON was intended to consume an amount of energy almost equal to the SALDO of PRO

$$A^{Imp}_{REF,CON} \sim \left(A^{Exp}_{REF,PRO} - A^{Imp}_{REF,PRO}\right). \tag{18}$$

The reference energy values (REFs) in the registers at the PoCs ($A^{Imp}_{REF,Z}$, $A^{Exp}_{REF,Z}$) were calculated from instantaneous voltage and current readings recorded by a 24 bit, 50 kHz DAQ system (DEWE-2600 using signal conditioning by the DEWE

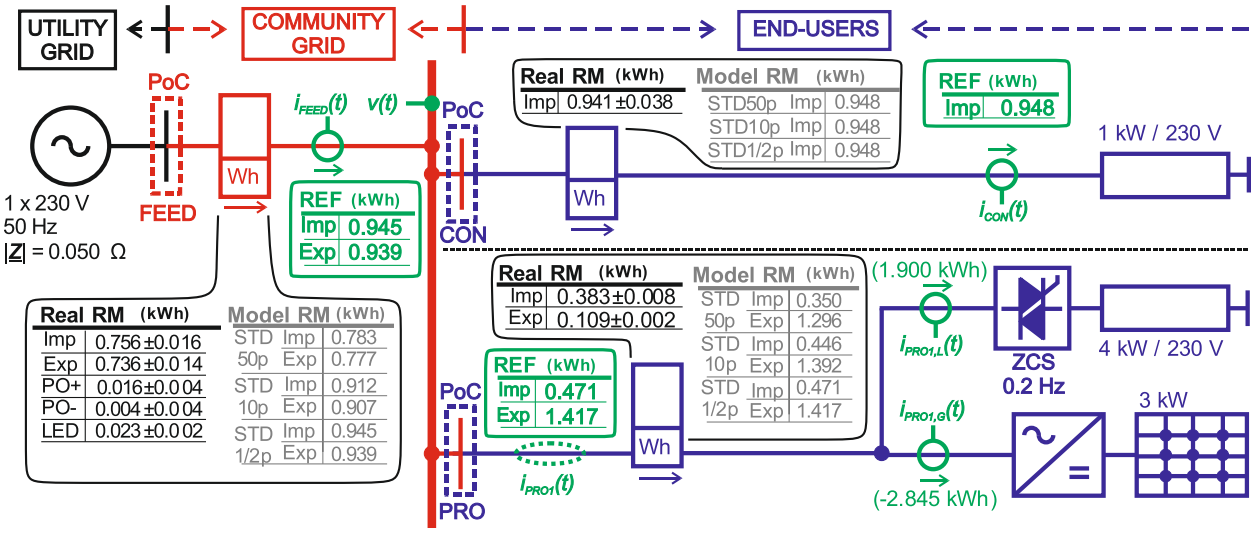

Fig. 10. Diagram of the single-phase testing community grid model with one prosumer (PRO) and one consumer (CON), connected to the utility grid, together with the energy values registered in real and model RMs, along with reference exported and imported energy values for $f_{sw} = 0.2$ Hz, i.e., $T_{sw} = 5$ s.

HSI/DAQP type of amplifier). Current $i_{FEED}(t)$ and $i_{CON}(t)$ were sensed using zero-flux transducers (DEWE PM-CM-60).

The active energy increment in kth interval $\Delta A^{Y}_{REF,Z}(k)$ is calculated using $T = T_{fund}/2$ in (1) and (2), and subsequently sorted to Imp and Exp and added to the cumulated energy according to (3) and (4). The readings of the real and modeled RMs, as well as the REF values, are reported in the corresponding tables within the figure.

It is possible to observe the following for the considered case:

1) At the PoC CON, all the readings correspond because the energy flow is unidirectional.
2) At the PoC PRO, the readings using STD50p and STD10p are different from both the real RM and REF readings, indicating that the real RM does not implement those metrics and creates a potential issue in terms of ambiguity.
3) At the PoC FEED, the readings using STD50p are very close to those of the real RM, indicating that this metric is implemented, but they are both different from REF. Moreover, the three readings of the individual outputs of the real RM are different from each other and thus do not comply with the standards.
4) In all cases, STD1/2p always gives results corresponding to REF, suggesting that the use of this metric is fair.

B. Individual RM Readings

Figs. 11 and 12 show readings relative to the REF values of the two real RMs installed at the PoC FEED and PoC PRO, respectively, under various tested T_{sw}. Again, as in Figs. 8 and 9, deviations in the normalized readings from one represent the errors of each metric under the specific test conditions. Based on the author's experience, the vast majority of rms implement the STD50p metric. Therefore, the graphs are supplemented with the theoretical deviations of the STD50p metric, according to Fig. 9, adapted to the ratio of the reference export and import energy values ($A^{Exp}_{REF,Z}/A^{Imp}_{REF,Z}$) for each T_{sw}. Fig. 11(a) and (b) shows that the RM's readings in the Imp/Exp

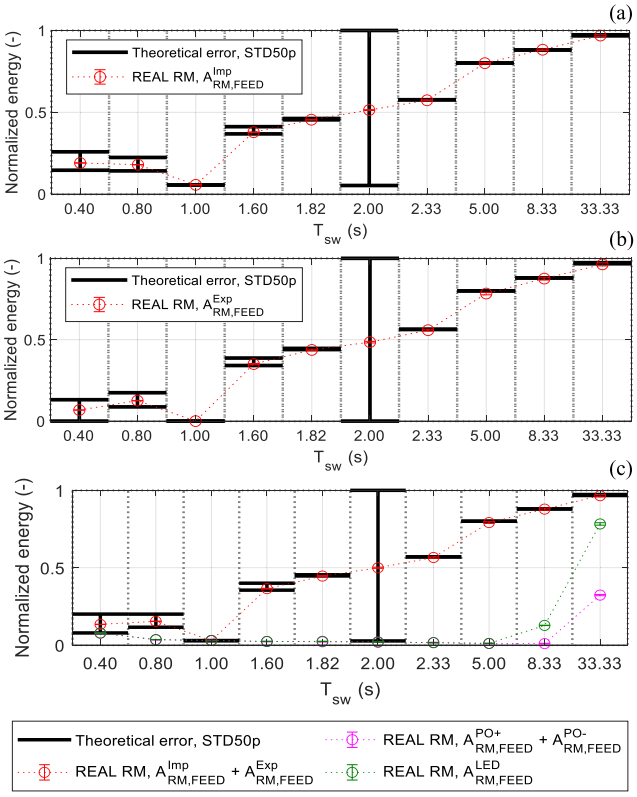

Fig. 11. Registered energy by means of the real RM and energy predicted by the STD50p model at the PoC FEED in (a) import and (b) export registers, and (c) the total amount of registered energy by the individual RM outputs.

registers, respectively, agree very well with the prediction from the model of the metric (STD50p).

Because the $A^{Exp}_{REF,Z}/A^{Imp}_{REF,Z}$ ratio was kept close to one for the individual experiments at the FEED point, the results for the Imp (a) and Exp (b) registers are almost equal.

Evidently, deviations in the registered energy values are acceptable if the changes in the P direction are less frequent than once per ~16 s (i.e., point with $T_{sw} = 33.33$ s). In order to compare the individual RM outputs (Imp/Exp; PO+/−; LED), the absolute sums of Imp and Exp, and PO+ and

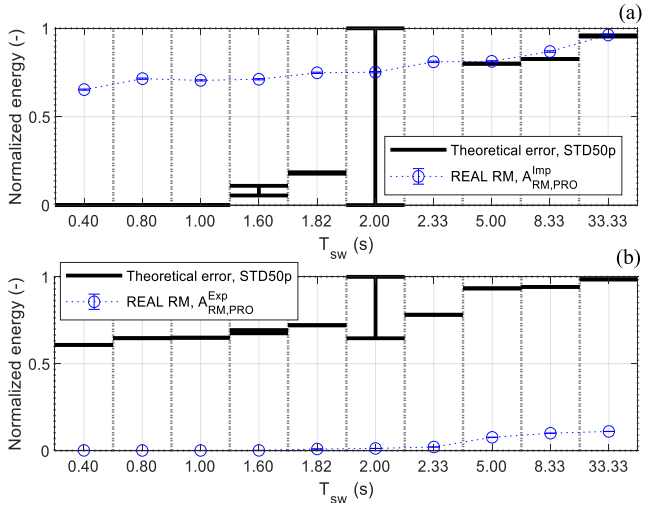

Fig. 12. Registered energy by means of the real RM and energy predicted by the STD50p model at the PoC PRO in the (a) import and (b) export registers.

TABLE I

TOTAL SALDO VALUES IN THE COMMUNITY GRID FOR DIFFERENT RMS AT DIFFERENT POCS

RM at PoC FEED	RM at PoC PRO	RM at PoC CON	SALDO (kWh)
REF	REF	REF	0.008
STD50p	STD1/2p	STD50p	0.008
STD1/2p	STD50p	STD50p	0.008
Real RM	Real RM	Real RM	1.234

PO−, respectively, are presented in Fig. 11(c), because the LED output exactly provides the absolute sum.

As indicated in Fig. 10, the e pulse outputs (electrical PO) and optical LED in Fig. 11(c) show more significant deviations and each is different from the other. This implies that the metrics of the RM's individual outputs are not the same, which is in contrast with the standard requirements.

Fig. 12(a) and (b) reports the RM readings the PoC PRO, where the $A^{Exp}_{REF,Z}/A^{Imp}_{REF,Z}$ ratio was kept close to three in all the individual experiments. Thus, the readings in the Imp and Exp registers have to be asymmetrical in favor of Exp, because the PRO is exporting. The comparison to the expected STD50p metric model response (from Fig. 9) shows a major discrepancy. In fact, the results for most tests do not match those of the STD50p metric, but they do not match the performance of any other examined metric either (Section III). The inconsistency is manifested by relatively small deviations in the Imp register, while a disproportionately small amount of energy is registered in the Exp register (consider that the PRO is a net exporter). Therefore, the measurement must be affected by another implementation aspect changing the behavior of the RM metric. Nevertheless, it is evidently shown that the metrics in the RMs at the PoC FEED and PoC PRO differ.

C. Community RM Readings

The results for imitated RMs in Fig. 10 (gray values) show individual deviations from REF (green values), with the deviation increasing with T_{MW}. Even when different simulated RMs were implemented at PoCs, the total SALDO (system losses) for the energy in the community grid (Table I), calculated based on the registered energy in the RMs (19), was the same as that for REF

$$\text{SALDO} = A^{Imp}_{X,PROS} + A^{Imp}_{X,CON} + A^{Imp}_{X,FEED} - A^{Exp}_{X,PROS} - A^{Exp}_{X,FEED}. \quad (19)$$

However, as the deviations of the simulated RMs change, issues with fair remuneration for the generated energy at the community level may arise if the price per kWh applied on the Imp and Exp registers differ. For example, if the RM at the PoC FEED implements the STD1/2p metric, the financial revenue for PRO depends exclusively on the metric implemented by the RM at the PoC PRO. However, the SALDO calculated from the readings of physical/real RMs (the black values in Fig. 10) significantly deviates from the reference SALDO, which is a consequence of the abnormal deviation exhibited by the RM at the PoC PRO (last row of Table I). It is therefore obvious that calculating the community grid losses using readings from rms exhibiting so-called abnormal deviations is nearly impossible.

However, the SALDO calculated from the readings of physical/real RMs (the black values in Fig. 10) significantly deviates from the reference SALDO, which is a consequence of the abnormal deviation exhibited by the RM at the PoC PRO (last row of Table I). It is therefore obvious that calculating the community grid losses using readings from rms exhibiting so-called abnormal deviations is nearly impossible. Conclusions are documented for one test ($f_{sw} = 0.2$ Hz, i.e., $T_{sw} = 5$ s) in Fig. 10. Conclusions for any other test point are essentially equivalent.

V. DISCUSSION AND RECOMMENDATIONS

The results discussed in the previous sections demonstrated that different metrics and different influencing factors/conditions can lead to large deviations in the RM readings. This applies both at the individual RM level (different outputs) and at the community network level (different RMs deployed).

The inability of RMs to correctly register and sort the active energy under fast/frequent changes in the power direction is related to the performance of the individual metrics. None of the five numerically and physically tested metrics, including their parametric sub-variants, could accurately indicate the true values for the imported and exported active energy if the direction changes were very frequent. However, the metrics gradually improved in their ability to measure and register correctly as the changes became less frequent (Fig. 8).

The experimental case study, supported by numerical analyses, highlighted the inconsistency of the energy balances in a community grid when different metrics are implemented in the RMs deployed at individual PoCs. Similar issues may be expected if the measurement windows of the RMs (relevant especially for the STD and FT metric-based RMs) are not synchronized, even if they are the same.

To avoid inadequate readings by the RMs with a mismatch between the energy produced and that consumed within a community grid, all the RMs have to use the same metric with the same parameterization. This recommendation is also valid for energy communities, where energy is traded via a utility grid. For this purpose, RM manufacturers should be required

to specify the type and parameterization of the metric used as part of the marking and documentation requirements [19].

Moreover, one of the RMs included in the experiment (RM at FEED PoC) exhibited a fundamental mismatch between the individual outputs [digital registers versus electrical pulse outputs versus metrological optical-LED output (Fig. 11)], while the other (RM at PRO PoC) showed a behavior not predictable by the metrics analyzed in this article under the considered conditions (Fig. 12). Considering practical circumstances, one option is to adopt a single metric suitable for these measurements and specify it in a standard assigned in static meter specifications (e.g., [18] and [20]) together with a set of type tests to verify their performances under frequent changes in the direction of the active energy flow (i.e., as in [19]). This is the approach used for power quality instruments, where the measurement methods are standardized (i.e., in IEC 61000-4-7/-15/-30), in order to prevent inconsistent results provided by individual instruments.

VI. Recommendation for a New Type Test

Recently, a new version of IEC 62052-11 [19] has been released, and a dynamic test targeting fast load current "unidirectional" variations (clause 9.4.12) has been newly introduced with "acceptance criterion A," which is devoted to testing for external influences on RMs under normal operating conditions characterized by a flow of energy different from zero. This test has also been accepted in the new edition of EN 50470-3 [18], where optional test parameters and acceptable limits of variation in the RM error are specified. The test prescribes periodic changes in time intervals t_{S1}, during which current I_{S1} is equal to I_n of DUT with displacement power factor $dPF = 1$, as specified in [18], and t_{S2}, during which current I_{S2} is zero. The duration times of these intervals are: 1) $t_{S1} = 10$ s, $t_{S2} = 10$ s; 2) $t_{S1} = 5$ s, $t_{S2} = 5$ s; and 3) $t_{S1} = 5$ s, $t_{S2} = 0.5$ s.

It seems feasible to adapt the procedure given in [19] for test 9.4.12 and extend it with test profiles corresponding to the addressed phenomenon (controlled "bidirectional" energy flows). Consequently, the particular requirements for test 9.4.12 in a relevant accuracy class standard (e.g., in [18]) could also be adopted for the proposed test. The proposed test aims to reveal the abnormal deviations and avoid different readings for the individual outputs (digital registers, optical and electrical pulse outputs) of a single RM. The intention is not to immediately disqualify the widely used RMs because no metric has yet been standardized. Therefore, no reference (standard meter) has been established for this influence.

A. Test Specification and Procedure

The absence of a standard meter capable of accurate measurements under frequent direction changes requires the use of a meter (DUT) test method based on a calibrator applying precisely specified test signals and a power-time measurement method [33].

Reference test conditions [19] should be ensured with the DUT voltage circuits energized with the highest specified nominal voltage. The objective of the current test signals proposed in this article is to use close timing for the two consecutive states, $S1$ and $S2$, which repeat as in 9.4.12 of [19]. However, modifications in the timing are required. In order to avoid the randomness of the STD metric theoretical error due to a time shift between the beginning of switching cycle and measuring window (T_{sh}/T_{MW} from Fig. 9 for STD50p), it is recommended to set T_{sw} (i.e., $t_{S1} + t_{S2}$) different from even a multiple of $T_{MW} = 1$ s. For ac tests, there is a need for synchronization with zero crossings of the main frequency, and an exact integral number of full fundamental cycles has to be applied for each state. This is conditional on the test method (i.e., the reference energy calculation). It also implies that the cycles have to be appropriately shifted for three-phase ac tests, as documented in Fig. 13.

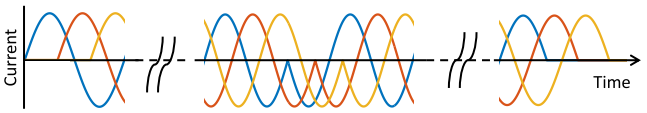

Fig. 13. Demonstration of test-current waveforms for a three-phase ac test.

TABLE II
Proposed Testing Signals

Test #	t_{S1} (s)	t_{S2} (s)	T_{sw} (s)	D (-)	I_{S1}	I_{S2}
①	25.5	25.5	51	0.5	$I_n\angle 0°$	$I_n\angle 180°$
②	5.5	5.5	11	0.5	$I_n\angle 0°$	$I_n\angle 180°$
③	5	0.5	5.5	0.909	$I_n\angle 0°$	$I_n\angle 180°$

TABLE III
Proposed Acceptable Limit of Variation in Error (%)

Test #	Meter's class [20]/ class index [18]		
	0,5/C	1/B	2/A
①	±1.0	±2.0	±3.0
②, ③	-	-	-

The parameters for the proposed test signals are summarized in Table II. Basically, cycle time T_{sw} is extended to 51 s, for test # ①, as the theoretical error from the true value drops down to 2% in the case of the STD50p metric (Fig. 8). This error value is actually 2/3 of the expected acceptable limit of variation in the error for a meter of class A (Table III). Therefore, the widely used RMs of class A employing the STD50p metric may pass. The test duration time, $\mathbf{t_D}$, at each test point should be selected so that the resolution error of the DUT registers and pulse outputs, at the same time, is less than 1% of the DUT accuracy class [33]. Moreover, the test duration time has to be an integral multiple of cycle time T_{sw}. The current in the first state, $S1$, is in phase with the voltage, while that in $S2$ has the opposite phase. It is recommended that current $I_{S1/S2}$ be equal to the RM nominal current (I_n), in consonance with [18] for test 9.4.12.

Based on Table II and considering the rest of the specification, reference active energy A in the import (+) and export (−) directions is calculated for each test point as follows:

$$A^{+}_{REF} = N_F \cdot V_n \cdot I_n \cdot \cos 0° \cdot t_{S1} \cdot N_C \quad (20)$$

$$A^{-}_{REF} = N_F \cdot V_n \cdot I_n \cdot \cos 180° \cdot t_{S2} \cdot N_C \quad (21)$$

where N_F, V_n, I_n, $t_{S1/S2}$, and N_C are the number of phases (1 or 3), nominal L-N RMs voltage, nominal RMs current, intervals from Table II and number of T_{sw} cycles in t_D, respectively.

Test ① is designed for "acceptance criterion A" [19] applicability with specifications for the acceptable limits of variation in the percentage error for RMs of common classes in Table III. The limits are adopted from [18] and [20] for test 9.4.12 and apply to the energy values registered in the Imp and Exp registers.

Following the guidance of Annex D in [33], the RM measurement error for active energy A_{RM}, in the import (+) and/or export (−) directions, is found as follows:

$$\delta A_{\mathrm{RM}}^{(+/-)} = \frac{|A_{\mathrm{RM}}^{(+/-)}| - |A_{\mathrm{REF}}^{(+/-)}|}{|A_{\mathrm{REF}}^{(+/-)}|} \cdot 100\% \tag{22}$$

where, in general, $(+/-) \in \{\mathrm{Imp}, \mathrm{Exp}, \mathrm{LED}, \mathrm{PO}+, \mathrm{PO}-\}$ denotes the examined RM output. If a single LED for A is employed, then $A_{\mathrm{REF}}^{(+/-)} = |A_{\mathrm{REF}}^{+}| + |A_{\mathrm{REF}}^{-}|$ is used, otherwise LED+ and LED− are examined separately. Consequently, the following condition regarding the acceptable variation limit specified by $\varepsilon_{\mathrm{VL}}$ (Table III) from accuracy class error limit $\varepsilon_{\mathrm{CL}}$ for the relevant accuracy class (numerically equal to the class, see Table III) has to be met:

$$|\delta A_{\mathrm{RM}}^{(+/-)}| \leq (|\varepsilon_{\mathrm{VL}}| + |\varepsilon_{\mathrm{CL}}|). \tag{23}$$

The method of extending the accuracy class limit by the acceptable variation limit corresponds to the method of setting the error limits for the influencing conditions.

On the other hand, shorter cycles for tests ② and ③ could actually disqualify today's RMs. Thus, the acceptance criteria of [19] and limits of Table III for ① are not applicable, until a standard metric is defined. Nevertheless, it is proposed to base the RM acceptance, for tests ② and ③, on the requirement of equal measured energy values at all corresponding outputs of a single RM (uniform metrics test), within a permissible error range. The difference limit is specified by [19] as ±1/10 of ε_{CL}. Because the energy is measured in both the import and export directions during a single test, possibly even asymmetrically, this implies the need for a hardware solution with two LEDs for import and export, in terms of the metrological pulse optical output.

The individual measurement errors are obtained using (22). Subsequently, the following condition regarding the acceptable difference limit determined by $\varepsilon_{\mathrm{CL}}$ has to be met:

$$\frac{|A_{\mathrm{RM}}^{1\mathrm{st}(+/-)}| - |A_{\mathrm{REF}}^{2\mathrm{nd}(+/-)}|}{|A_{\mathrm{REF}}^{(+/-)}|} \cdot 100\% = |\delta A_{\mathrm{RM}}^{1\mathrm{st}(+/-)} - \delta A_{\mathrm{RM}}^{2\mathrm{nd}(+/-)}| \leq |\varepsilon_{\mathrm{CL}}|/10 \tag{24}$$

where $1\mathrm{st}(+/-) \neq 2\mathrm{nd}(+/-)$, e.g., Imp and PO+ are compared.

B. Application of the Proposed Test

Three certified RMs were selected to cover multiple classes (A and B) and implement various metrics. An overview of these RMs is provided in Table IV.

Tests were performed consecutively as described in Section V-B for RM1 to RM3 and tests ① to ③. The test setup is shown in Fig. 14. The calibrator used was a calibrated Omicron CMC 256 plus unit, generating test signals according to the specification discussed in Section V-B. The pulse outputs of the RM were sensed by the digital inputs of an NI USB 6009 card equipped with a photo-transistor switch for optical pulse output sensing. The pulse counter was subsequently implemented using software (LabVIEW) in the control PC.

At the end of each test, the registered corresponding active energy values (Imp, Exp) and pulses converted to energy (by means of the number of pulses, N_P, registered and RM pulse constant c from Table IV, i.e., $A = N_P/c$) were collected and processed to determine the errors by means of (22). Finally, the measurement errors were compared with the error limits in terms of (23) and (24). The results are reported in Table V.

The uncertainties of the RM readings were determined in accordance with [33] Annex D. However, for the purpose of

TABLE IV
TESTED SAMPLES OF RMS

RM	System	V_n (V)	I_n (A)	Acc. class [18]	LED (1/kWh)		PO (1/kWh)	
					(+)	(-)	(+)	(-)
RM1	3ph (L-N)	230	5	A	500 [1)]		250	250
RM2	3ph (L-N)	230	5	B	1000 [1)]		295	295
RM3	3ph (L-N)	230	5	B	2500	2500	-	-

[1)] a single LED processing pulses in both directions, i.e., |(+)| + |(−)|

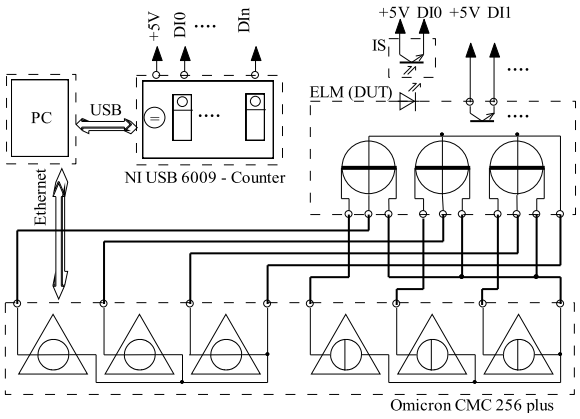

Fig. 14. Test setup.

TABLE V
TESTS RESULTS

RM | Test # | direction			A_{REF} (Wh)	$\delta A_{RM}^{Im./Ex.}$ (%)	δA_{RM}^{LED} (%)	δA_{RM}^{PO} (%)	u (%)	Pass/ Fail
RM1	①	(+)	2541,5	**-2,03**	-7,06	-12,34	±0.14	**P**
		(-)	-2541,5	**-1,99**		-12,34	±0.14	**P**
	②	(+)	2319,2	**-9,15**	**-42,13**	**-60,16**	±0.14	**F**
		(-)	-2319,2	**-9,11**		**-60,16**	±0.14	**F**
	③	(+)	38333	**-10,07**	**-18,34**	**-10,18**	±0.14	**P**
		(-)	-3833,3	**-99,69**		**-100,00**	±0.14	**F**
RM2	①	(+)	3812,3	**-1,97**	-2,03	-2,01	±0.14	**P**
		(-)	-3812,3	**-1,97**		-1,92	±0.14	**P**
	②	(+)	3478,8	**-9,13**	**-9,13**	**-9,18**	±0.14	**P**
		(-)	-3478,8	**-9,08**		**-9,08**	±0.14	**P**
	③	(+)	63490	**-10,03**	**-18,20**	**-10,01**	±0.14	**P**
		(-)	-6349,0	**-99,64**		**-99,68**	±0.14	**P**
RM3	①	(+)	2688,1	**-0,08**	-0,06	-	±0.14	**P**
		(-)	-2688,1	**-0,15**	-0,15	-	±0.14	**P**
	②	(+)	2740,8	**-0,07**	**-0,06**	-	±0.14	**P**
		(-)	-2740,8	**-0,18**	**-0,15**	-	±0.14	**P**
	③	(+)	46958	**-0,06**	**-0,06**	-	±0.14	**P**
		(-)	-4695,8	**-0,19**	**-0,18**	-	±0.14	**P**

this first application, only the contribution of the calibrator was taken into account because the tests were conducted only once. The Type B standard uncertainty was based on the manufacturer's calibrator accuracy specifications and equations (20) and (21). In order to obtain the expanded uncertainty, a factor of 2 was used. In general and in relative form, the extended uncertainty is found as follows:

$$u^{(+/-)} = \left(2 \cdot \sum_{\forall x \in X} \left| \frac{\partial A_{\mathrm{REF}}^{(+/-)}}{\partial x} \right| \cdot \frac{\varepsilon_x}{\sqrt{3}} \right) / A_{\mathrm{REF}}^{(+/-)} \cdot 100\% \quad (25)$$

where $X = \{V_n, I_n, \varphi, t\}$ and the individual error limits for CMC256+ under the test conditions (230 V, 5 A) are as follows: $\varepsilon_V = \pm 0.12$ V, $\varepsilon_I = \pm 3.3$ mA, $\varepsilon_\varphi = \pm 0.35$ mrad, $\varepsilon_t = \pm 1.5$ppm. The uncertainties for each test performed are included in Table V. The pass or fail statement is expressed as a logical AND of the individual conditions of the corresponding row involving results, i.e., errors, in bold.

In consistency with the influencing condition, it can be observed that all tested RMs underestimate the measured energy (negative errors), however, they all satisfy the proposed test ① . In the case of RM1 and RM2, the errors of their registers match the theoretical assumptions for a window-based metric with a length of 50 periods (i.e. STD50p or FT50p, see Section III). On the other hand, the RM3 clearly uses a much faster metric that shows minimal error for all tests. The pulse outputs of RM2 and RM3 are consistent with the registers, so in this respect the given RMs are also satisfactory. While for the RM1, the correlation differences between all individual outputs for tests ② and ③ are outside the error limit, nonconforming. This points to inconsistent metrics of individual outputs for the RM1. It can be concluded that the tests are designed correctly as intended.

VII. Conclusion

This article analyzed the ability of RMs to properly detect between imported and exported energy values under dynamic changes in the power direction and presented the possible consequences of incorrect readings on energy trading in community grids.

Five types of active power and energy metrics used in RMs or derived from other applications of active power measurement were reviewed, and the sensitivity to their parametric modifications was analyzed when exposed to synthetic periodic changes in the active power direction. The numerical analysis revealed limitations in the measurements of window-based metrics because they primarily reflect the average transmitted energy during the measurement window. Metrics that demonstrated better performances were those capable of providing active power and energy increments after each sample of the input signals, although some levels of error were still observed. The impacts of other influencing factors such as the frequency of the changes and exported to imported energy ratio were also evaluated in a detailed analysis of window-based metrics, which gave a comprehensive theoretical background for the deviation of the most commonly used RMs.

The experimental part of the article demonstrated that the deployment of RMs implementing different metrics at grid PoMs may cause unfair remuneration of net exporting prosumers, when a generating plant simultaneously operates with cycle-controlled loads. Moreover, the experiment showed that commercial RMs, even if passing all the standardized metrological tests, may be completely inappropriate for use, because they exhibit deviations from different origins in each register. Consequently, it was demonstrated that the calculation of the technical losses in the microgrid is nearly impossible. To prevent RMs from similar behavior, a new testing procedure, supplementing the current standard tests, was designed, experimentally evaluated, and proposed to be included in relevant standards update.

It is important to note that this study exclusively focused on the metrics used for the measurement of active power and energy from the perspective of real energy exchange among community actors and between a community and DSs, using numerical simulations and controlled laboratory experiments, under simplified conditions. Other influencing factors such as simultaneous distorted current drawn by non-linear loads in the prosumer installation and/or background voltage distortion will be the subject of further theoretical and experimental studies, while also taking into account the uncertainties related to the measuring chain.

Acknowledgment

This research work has been carried out at the Centre for Research and Utilization of Renewable Energy (CVVOZE).

References

[1] K. Weranga, S. Kumarawadu, and D. P. Chandima, "Evolution of electricity meters," in *Smart Metering Design and Applications*. (SpringerBriefs in Applied Sciences and Technology). Singapore: Springer, 2014, doi: 10.1007/978-981-4451-82-6_2.

[2] *Handbook for Electricity Metering*, 10th ed. Edison Electrical Institute, Washington, DC, USA, 2002.

[3] J. Drapela, J. Moravek, L. Radil, and P. Mastny, "Performance of standard power/energy metric under fast changes in active energy flow direction," in *Proc. 19th Int. Conf. Harm. Quality Pow. (ICHQP)*, 2020, pp. 1–6, doi: 10.1109/ICHQP46026.2020.9177900.

[4] J. Klusacek, M. Vrana, J. Drapela, J. Moravek, and P. Mastny, "Advanced design of heat accumulation responsive demand control for energy management of prosumers," in *Proc. 26th Int. Conf. Exhib. Electr. Distrib. (CIRED)*, vol. 2021, Sep. 2021, pp. 986–990, doi: 10.1049/icp.2021.1562.

[5] H. Zhu, K. Ouahada, and A. M. Abu-Mahfouz, "Peer-to-peer energy trading in smart energy communities: A Lyapunov-based energy control and trading system," *IEEE Access*, vol. 10, pp. 42916–42932, 2022, doi: 10.1109/ACCESS.2022.3167828.

[6] D. Kanakadhurga and N. Prabaharan, "Demand side management in microgrid: A critical review of key issues and recent trends," *Renew. Sustain. Energy Rev.*, vol. 156, Mar. 2022, Art. no. 111915, doi: 10.1016/j.rser.2021.111915.

[7] J. Moravek, J. Drapela, V. Wasserbauer, and P. Mastny, "Power quality issues related to power flow control in systems with renewable energy micro sources," in *Proc. 17th Int. Sci. Conf. Electr. Power Eng. (EPE)*, May 2016, pp. 1–6, doi: 10.1109/EPE.2016.7521784.

[8] M. Vojtek, J. Drapela, P. Mastny, J. Moravek, M. Vrana, and J. Klusacek, "Analysis and verification of operating characteristics of hybrid inverter with external power meter," in *Proc. 22nd Int. Sci. Conf. Electr. Power Eng. (EPE)*, Kouty nad Desnou, Czech Republic, Jun. 2022, pp. 1–5, doi: 10.1109/EPE54603.2022.9814096.

[9] Z. Dalala, T. Alwahsh, and O. Saadeh, "Energy recovery control in elevators with automatic rescue application," *J. Energy Storage*, vol. 43, Nov. 2021, Art. no. 103168, doi: 10.1016/j.est.2021.103168.

[10] A. T. H. T. Anh and L. H. Duc, "A regenerative braking energy recuperation from elevator operation in building by active rectifier," *Int. J. Power Electron. Drive Syst. (IJPEDS)*, vol. 12, no. 2, p. 811, Jun. 2021, doi: 10.11591/ijpeds.v12.i2.pp811-821.

[11] G. Barone et al., "How smart metering and smart charging may help a local energy community in collective self-consumption in presence of electric vehicles," *Energies*, vol. 13, no. 16, p. 4163, Aug. 2020, doi: 10.3390/en13164163.
[12] M. Anda and J. Temmen, "Smart metering for residential energy efficiency: The use of community based social marketing for behavioural change and smart grid introduction," *Renew. Energy*, vol. 67, pp. 119–127, Jul. 2014, doi: 10.1016/j.renene.2013.11.020.
[13] M. Orlando et al., "A smart meter infrastructure for smart grid IoT applications," *IEEE Internet Things J.*, vol. 9, no. 14, pp. 12529–12541, Jul. 2022, doi: 10.1109/JIOT.2021.3137596.
[14] G. Artale et al., "PQ metrics implementation on low cost smart metering Platforms. A case study analysis," in *Proc. IEEE 9th Int. Workshop Appl. Meas. Power Syst. (AMPS)*, Bologna, Italy, Sep. 2018, pp. 1–6, doi: 10.1109/AMPS.2018.8494866.
[15] J. Klusacek, J. Drapela, and R. Langella, "Revenue metering of unbalanced prosumers in energy communities," *IEEE Open Access J. Power Energy*, vol. 10, pp. 426–437, 2023, doi: 10.1109/OAJPE.2023.3243385.
[16] EU Directive on Measuring Instruments (MID), *European Parliament and of the Council*, document 2014/32/EU, 2014.
[17] *Electricity metering Equipment (A.C.)—Part 1: General Requirements, Tests and Test conditions—Metering Equipment (Class Indexes A, B and C)*, document EN 50470-1:2006, 2006.
[18] *Electricity Metering Equipment—Part 3: Particular Requirements—Static Meters for AC Active Energy (Class Inx. A, B and C)*, document EN 50470-3:2022, 2022.
[19] *Electricity Metering Equipment—General Requirements, Tests and Test Conditions—Part 11: Metering Equipment*, document IEC 62052-11:2020, 2020.
[20] *Electricity Metering Equipment—Particular Requirements—Part 21: Static Meters for AC Active Energy (Classes 0,5, 1 and 2)*, document IEC 62053-21:2020, 2020.
[21] *Electricity Metering Data Exchange—The DLMS/COSEM Suite—Part 6-1: Object Identification System (OBIS)*, document IEC 62056-6-1:2017, 2017.
[22] R. Q. Cetina, A. J. Roscoe, and P. S. Wright, "A review of electrical metering accuracy standards in the context of dynamic power quality conditions of the grid," in *Proc. 52nd Int. Universities Power Eng. Conf. (UPEC)*, Heraklion, Greece, Aug. 2017, pp. 1–5, doi: 10.1109/UPEC.2017.8231871.
[23] L. Bartolomei, D. Cavaliere, A. Mingotti, L. Peretto, and R. Tinarelli, "Testing of electrical energy meters subject to realistic distorted voltages and currents," *Energies*, vol. 13, no. 8, p. 2023, Apr. 2020, doi: 10.3390/en13082023.
[24] J. Novotny, J. Drapela, and D. Topolanek, "Frequency response of revenue meters in measured active energy," in *Proc. 17th Int. Conf. Harmon. Quality Power (ICHQP)*, Belo Horizonte, Brazil, Oct. 2016, pp. 524–529, doi: 10.1109/ICHQP.2016.7783309.
[25] A. Bernieri, G. Betta, L. Ferrigno, M. Laracca, and R. S. L. Moriello, "Electrical energy metering: Some challenges of the European directive on measuring instruments (MID)," *Measurement*, vol. 46, no. 9, pp. 3347–3354, 2013, doi: 10.1016/j.measurement.2013.06.025.
[26] B. T. Have, T. Hartman, N. Moonen, and F. Leferink, "Static energy meters and the electrical environment comply to the standards but are not compatible," *IEEE Electromagn. Compat. Mag.*, vol. 12, no. 1, pp. 59–68, 1st Quart. 023, doi: 10.1109/MEMC.2023.10135174.
[27] H. K. M. Paredes, F. P. Marafão, P. Mattavelli, and P. Tenti, "Application of conservative power theory to load and line characterization and revenue metering," in *Proc. IEEE Int. Workshop Appl. Meas. Power Syst. (AMPS)*, Aachen, Germany, Sep. 2012, pp. 1–6, doi: 10.1109/AMPS.2012.6343993.
[28] M. Mienkina, "Filter-based algorithm for metering applications," NXP Semiconductors, Eindhoven, The Netherlands, Appl. Note AN4265, Apr. 2016.
[29] *ADE 7758' Poly Phase Multifunction Energy Metering IC with Per Phase Information*, Data Sheet, Analog Devices, Wilmington, MA, USA, 2011.
[30] F. Blaabjerg, *Control of Power Electronic Converters and Systems*. New York, NY, USA: Academic, 2018, doi: 10.1016/B978-0-12-805245-7.09989-3.
[31] J. Klusacek, J. Drapela, R. Langella, and J. Meyer, "Revenue Metrics Ability to Correctly Register Bidirectional Active Energy Flows in Active Distribution Networks," in *Proc. IEEE 13th Int. Workshop Appl. Meas. Power Syst. (AMPS)*, Bern, Switzerland, Sep. 2023, pp. 01–06, doi: 10.1109/AMPS59207.2023.10297185.
[32] *Electricity Metering—Data Exchange for Meter Reading, Tariff and Load Control—Part 21: Direct Local Data Exchange*, document IEC 62056-21:2002, 2002.
[33] *Electrical Energy Meters—Test Equipment, Techniques and Procedures—Part 1: Stationary Meter Test Units (MTUs)*, document IEC 62057-1:2023, 2023.

Jan Klusacek (Student Member, IEEE) received the M.Sc. degree in electrical power engineering from Brno University of Technology, Brno, Czech Republic, in 2020, where he is currently pursuing the Ph.D. degree with dissertation topic "Definition and Measurement of Electrical Power Components in Future Distribution Systems."

His research interests include power measurement, power quality in active distribution systems, power converters and coordination of distributed generators, and active loads.

Roberto Langella (Senior Member, IEEE) was born in Naples, Italy, in March 1972. He received the Laurea degree in electrical engineering from the University of Naples, Naples, in 1996, and the Ph.D. degree in electrical energy conversion from the University of Campania "Luigi Vanvitelli," Aversa, Italy, in 2000.

He is currently a Full Professor of electrical power systems with the University of Campania "Luigi Vanvitelli."

Dr. Langella is the Chair of the IEEE PES TF on Harmonic Modeling, Simulation, and Assessment.

Jan Meyer (Senior Member, IEEE) received the Dipl.-Ing. and Ph.D. degrees in electrical power engineering and postdoctoral qualification in power quality from TUD Dresden University of Technology, Dresden, Germany, in 1994, 2004, and 2018, respectively.

He was appointed as a Professor for "Power Quality" in 2022 and is the Team Leader of the Power Quality Research Group, TUD Dresden University of Technology. His research interests include measurement, modeling and simulation of network disturbances, especially distortion below and above 2 kHz, all aspects related to the uncertainty in power quality measurements as well as the efficient and automated analysis of large data amounts from power quality measurement campaigns.

Dr. Meyer is a member of several national and international working groups on EMC standardization. He is the Co-Chair of German EMC Committee DKE U.K. 767.1. He is active in several CIGRE and IEEE working groups as well as the CIRED TC. He regularly gives invited speeches and organizes tutorials, panels, and workshops in the field of power quality.

Jiri Drapela (Senior Member, IEEE) received the M.Sc. and Ph.D. degrees in electrical power engineering from Brno University of Technology, Brno, Czech Republic, in 1999 and 2006, respectively.

He is currently with Brno University of Technology as a Full Professor of power systems and the Team Leader at the Power Quality Research Group. His research interests include power quality and power network conducted disturbances, especially immunity, emission of electrical appliances, and power quality measurement techniques.

Open Access funding provided by 'Università degli Studi della Campania "Luigi Vanvitelli"'
within the CRUI CARE Agreement